Implicit and explicit solvent models for modelling a bifunctional arene ruthenium hydrogen-storage catalyst: a classical and *ab initio* molecular simulation study

Sateesh Bandaru[1,2,b)], Niall J. English[1,2 ,a)] and J.M.D. MacElroy[1,2]

[1]*The SFI Strategic Research Cluster in Solar Energy Conversion,* [2]*School of Chemical and Bioprocess Engineering,*

University College Dublin, Belfield, Dublin 4, Ireland.

Classical and *ab initio*, Density Functional Theory (DFT)- and semi-empirical-based molecular simulation, including molecular dynamics (MD), have been carried out to compare and contrast the effect of explicit and implicit solvation representation of tetrahydrofuran solvent on the structural, energetic and dynamical properties of a novel bifunctional arene ruthenium catalyst embedded therein. Particular scrutiny was afforded to hydrogen-bonding and energetic interactions with the THF liquid. It was found that the presence of explicit THF solvent molecules is required to capture an accurate picture of the catalyst's structural properties, particularly in view of the importance of hydrogen bonding with the surrounding THF molecules. This has implications for accurate modelling of the reactivity of the catalyst.

[a] Corresponding authors. Email: [a)] niall.english@ucd.ie, [b)] sateesh.bandaru@ucd.ie

Introduction

A plethora of important organic and organo-metallic reactions take place in the liquid phase. Indeed, in the 1860's, Berhelot and St. Gilles showed that the rates of homogeneous chemical reactions depend considerably on the environment.[1] The rates of reaction and reactivity of polar systems, and also of catalyst efficacy, depend crucially on the solvent environment; this is especially so when polar transition states are involved, and rates and catalytic effectiveness can vary many orders of magnitude depending on the solvent.[2] Therefore, any *in silico* molecular-simulation attempts to model chemical reactivity in the liquid phase need to examine and validate carefully the apposite treatment of the solvent concerned, quite apart from gauging any underlying, non-directly-chemical effects on the species and any catalysts involved, *e.g.*, structural and dynamical properties thereof. Theoretically, solvent effects may be modelled in two ways: by explicit representation and implicitly by continuum representation, e.g., dielectric Polarisable Continuum Model (D-PCM)[3] and conductor-like PCM (C-PCM)[4] in the context of a Density Functional Theory (DFT) treatment, and also the Poisson-Boltzmann[5] or Generalised Born solvation[6] approach for a classical molecular simulation representation. An explicit representation allows for direct interaction of the species with the solvent molecules. Implicit solvation, in which a polar solute polarises the surrounding dielectric medium, allows for some dipolar interactions with the solvent to be represented by proxy in a crude manner, whereas many important features of interaction with the solvent are lost, *e.g.*, hydrogen-bonding; this has a very direct negative, and often crucial, bearing on accurate representation, often qualitatively so, on the structural, dynamical, energetic and chemical-reactivity properties of the solute.[7]

Theoretically, one may study these solute-solvent interactions using quantum mechanical (QM) methods, *e.g.*, DFT, or classical molecular simulation, *e.g.*, molecular dynamics (MD);[8] also possible are mixed quantum-classical methods (QM/MM),[9] but linear-scaling DFT methods are becoming comparatively more attractive in this latter respect.[10] In the traditional QM approach, it is computationally and operationally prohibitive to model more than a very limited number of solvent molecules interacting with the solute; this approach means that second or successive coordination 'layers' of solvent molecules cannot be realistically models (under the perhaps heroic assumption that a primary layer can even be represented explicitly); even so, DFT functionals have their own drawbacks *per se* and are often *sui generis* for accurate representation of specific classes of compunds. In contrast, QM/MM and MD allow *ipso facto* for the modelling of thousands of atoms, despite the very serious

underlying problems of QM/MM (notwithstanding its operational deployment) and the difficulties of DFT in handling dispersion accurately, coupled with the inability of classical simulation to handle chemical adsorption and its need for laborious *ab origine* parameterisation.

Organo-ruthenium catalysts play very important roles, such as cross metathesis, ring-opening metathesis polymerisation (*e.g.*, in the sense of Grubbs first-generation catalysts),[11] ring-closing metathesis (à la Grubbs second-generation catalysts), hydrogenation, cross-coupling and olefin isomerisation. In recent years, many novel ruthenium catalysts have been designed for hydrogen storage in ammonia boranes.[12,13] A great number of highly active organo-ruthenium catalysts have been applied to dehydrocoupling reactions of ammonia borane and related boron-nitride substrates.[14-18] Most of these reactions use tetrahydrofuran (THF) as a solvent; it is aprotic with a dielectric constant of $\varepsilon = 7.6$. THF can be used in hydroboration reactions, and as a solvent for organo-metallic compounds. Although similar to diethyl ether, THF acts as a stronger base. It is moderately polar and can dissolve a wide range of nonpolar and polar chemical compounds.[19]

Motivated by our interest in catalysed chemical hydrogen storage, in particular the recent study of a novel bifunctional arene ruthenium catalyst of Schreiber *et al* for highly efficient H_2 dehydrocoupling of ammonia boranes (detailed in Scheme 1),[12] our primary goal in this study is a detailed comparison of implicit and explicit solvent representation of THF effects on the structural, energetic and dynamical behaviour of this catalyst. We also examine the effects of incorporating explicit solvation on the reaction cycle, whilst focussing the structure **1** in Scheme 1. We carried out classical MD simulations under periodic boundary conditions (PBC) of the catalyst in THF, and sampled ten representative configurations of the catalyst with its immediate solvation layer therefrom for further DFT-based analysis, including *ab initio* molecular dynamics (AIMD) with a semi-empirical Hamiltonian. We probed the structural, energetic and dynamical properties of the catalyst, as well as interactions with the solvent, and compared this to an *in vacuo*, gas-phase representation as well as using continuum solvation in DFT.

[insert Scheme 1 about here]

Methodology

Given the Ru atom and challenges for its force-field parameterisation, coupled with the cationic nature of the catalyst,[12] it is necessary to use semi-empirical partial charges for a subsequent force-field based representation, owing to a paucity of available reliable 'dictionary-based' partial charges. Using the MOE software package,[20] point charges were computed for the catalyst (structure **1** in Scheme 1) following geometry optimisation *in vacuo* with the conjugate gradient method from the X-ray structure,[12] via AM1-BCC in MOPAC. The AMBER 99 force-field[21] was then used to model this catalyst structure with the AM1-BCC charges, with which they are consistent. Non-bonded interactions were treated using a twin-range method,[22] with a short and long cut-off radius of 18 and 20 Å, respectively; the relatively large values were chosen due to the cationic nature of the catalyst. The reaction field method[23] was used to handle long-range electrostatics, and the dielectric constant set at the experimental value of 7.6.[19] In order to assess size dependence of the solute-solvent interaction, the catalyst was placed in the centre of two cubic periodic boxes containing 1,000 and 512 THF molecules relaxed via MD in the liquid state at 330 K and 1 atm. THF molecules were then removed if their constituent atoms were less than 2.8 Å in distance from the heavy atoms of the catalyst, leaving 963 and 487 THF molecules, respectively, under PBC.[8] Prior to MD under PBC, the heavy atoms in the simulation boxes were fixed and the system was relaxed by energy minimisation using a composite protocol of steepest descent (SD), conjugate gradient (CG) and truncated Newton (TN) steps, with respective termination gradients of 1000, 100 and 10 kcal/mol·Å. Preliminary relaxation simulations were carried out in the NPT ensemble after the energy minimisation described above and bond lengths were constrained with a relative tolerance of 10^{-7};[8] these simulations were carried out until the system volumes stabilised and then continued for a further 0.15 ns. A timestep of 1 fs was used. This was assessed for energy conservation in the NVE ensemble after the NPT relaxation simulations and was found to be satisfactory: the percentage relative drift in energy, defined as the ratio of the energy drift (expressed as a linear regression coefficient) to the average kinetic energy during the simulation,[24] was less than 0.5 % over 50 ps for the relaxed PBC systems in both cases. The periods of the thermal and barostat reservoirs[8] were set to 0.5 and 2 ps, to allow for relatively weak coupling. The solute-solvent interaction energies, in terms of both van der Waals and Coulombic components, were computed in both of the systems and compared over the latter 0.15 ns period of NPT relaxation (*post* volume-stabilisation); it was found that these were comparable. Therefore, this indicates that the use

of the smaller system is permissible for full production simulation. 0.5 ns of NPT production simulation was carried out subsequently for the smaller system. The probability distribution of the solute-solvent interaction energies were extracted from the trajectory *ex post facto*, and ten configurations were chosen from the therefrom to represent the (essentially Gaussian) spread thereof. Of these (PBC) configurations, the catalyst and the primary coordination layer of THF molecules were taken; in practice, this led to retaining the nearest six THF molecules. These snapshots were then used for subsequent DFT-based geometry optimisation and AIMD; naturally, conventional, cubic-scaling, Gaussian-based DFT would be unable to handle such PBC systems of this size.

These ten 'stripped' solvated configurations were optimised using the hybrid meta-GGA M06L functionals[25,26] of Truhlar and co-workers, in the Gaussian 09 program package.[27] The Ru atom was represented by the Stuttgart/Dresden effective core potential and associated basis set, SDDAll[28] as implemented in Gaussian 09. A 6-31+G(d) + SDDAll mixed basis set was applied, employing the Stuttgart potential to Ru, whilst the remaining C, N, O, H atoms were modelled using Pople-type basis sets. These optimised configurations are available as Supplementary Information. Following geometry optimisation, frequency calculations were also carried out on the optimised geometries to estimate the nature of the stationary points. We have calculated the interaction energies of the solvent molecules with the catalyst, by calculating the difference between the energies of isolated moieties and their 'complex'. In our case we have treated all six solvent molecules as a single assembly and catalyst treated as another 'motif' or 'scaffold'. For both gas-phase and PCM treatments, single-point energy calculations were undertaken on the gas-phase-optimised configurations; the interaction energy was computed by subtracting the energies of the separate assemblies of THF and catalyst from that of the solute-THF complex. Comparison of the PCM result for the interaction energy with that computed *in vacuo* allows for the effect of solvation energetics beyond the first layer to be gauged, notwithstanding the obvious problem that the underlying geometry from optimisation in only six molecules of the first solvation layer may lead to less accurate results than that conducted in an full simulation box using PBC (although this would be prohibitive without linear-scaling DFT methods).

Ab initio MD simulations were carried out in the canonical ensemble[8] at 330 K using atom-centred density matrix propagation (ADMP)[29-32] starting with each M06L-optimised geometry of the catalyst-solvent complex, *i.e.*, ten independent AIMD simulations were

performed. The semi-empirical PM6 Hamiltonian[33] was used, with a time step of 0.5 fs and velocity-rescaling, for 5 ps, to allow for sampling of vibrational behaviour. AIMD was also carried out for the isolated catalyst, without solvent, as an *in vacuo* reference.

Results & Discussions

As mentioned previously, there were six THF molecules around the catalyst sampled in each of the ten representative configurations from classical MD. The interaction energies are presented in Table 1 from classical MD, specifying the van der Waals and Coulombic components, for both the six nearest THF molecules in the first coordination layer (on a non-PBC basis, akin to the subsequent DFT procedure on these configurations), as well as these components for the interaction with the entire set of THF molecules in the system (on a PBC basis, as is only appropriate). In each case, the reaction field method was used. In addition, the Generalised Born solvation method[6] was used to compute the electrostatic component of the interaction energy with the continuum solvent (with the catalyst in its solvated configuration, but stripped of all surrounding THF molecules); this ensures good convergence in the estimate of this component, the lack of which dogs Coulombic interaction energy estimation for explicit solvation.[34] As can be seen readily from Table 1, there is a marked difference in interaction energies upon the inclusion of THF molecules beyond the first solvation layer; such a difference is especially evident for the van der Waals term; this underlines dramatically the problem of truncating the solvation layer around a solute. Perhaps the most expedient and accurate approach to gauge the interaction energy with the solvent is to use the well-converged van der Waals component on a system-wide, PBC basis (capturing non-Coulombic interactions), in conjunction with the Born electrostatic term for the catalyst stripped of all THF molecules. This term is specified on the right of Table 1.

[insert Table 1 about here]

The interaction energies on the DFT-optimised configurations are presented in Table 2, along with the root mean square deviations (RMSD) of the catalyst with respect to the lowest-energy configuration (# 4). It was found that optimisation led to the adoption of sometimes-rather different configurations to those from classical MD; the somewhat marked

differences in RMSD values show this clearly, along with the substantially greater spread and variety in interaction energies as compared to the classical-simulation results in Table 1. It would appear that the PCM contribution to the solvation energy beyond the interaction energy with the immediate six THF neighbours, is in the 16-23 kcal/mol range, whilst the classical-simulation analogue is around 27-30 kcal/mol, from comparison of the electrostatic Born solvation energy term with that of the (PBC) explicit solvation term (cf. Table 1). Naturally, this is a very large energy adjustment that implicit solvation alone simply cannot capture, let alone neglecting entirely important non-bonded contacts and hydrogen-bonding arrangements with the surrounding solvent. Hydrogen bonds were defined such that the distance between the carbon atom of the catalyst and the oxygen atom in the THF was less than 4 Å and the C-H….O angle was greater than 140º. It was found that there was a wide variety of different placements and angular orientations of the THF molecules with respect to the catalyst 'scaffold', often governed by various different hydrogen bonding arrangements and other non-bonded contacts. To illustrate the rich variety of such contacts, each of the optimised conformations are depicted in Fig. 1, illustrating hydrogen bonding contacts. The persistence time of hydrogen bonds was found to be in general in the 0.1-1 ps range; such hydrogen bonds may break up and reform repeatedly; in a sense, this is a product of using a perhaps slightly crude pure geometric definition.

[insert Fig. 1 and Table 2 about here]

Considering more closely the conformations with the largest and smallest magnitudes of interaction energy (# 4 and 5, respectively) as examples, Fig. 2 illustrates these, along with the conformation achieved by gas-phase optimisation in the absence of any explicit solvent (cf. Fig. 2a). Fig. 2b depicts the structure with largest-magnitude interaction energy (# 4), which has a 'half-chair' shape, and a 'boat-shaped' configuration in Fig. 2b for the structure with the smallest-magnitude interaction energy (i.e., # 5). Naturally, it is clear that the absence of any explicit THF molecules results in important hydrogen-bonding and other important non-bonded contacts being missed altogether, which leads to a less realistic structure. A typical representation of the rich tapestry of time-behaviour of hydrogen bonds of a single THF molecule in close contact is depicted in Fig. 3 for the lowest-energy, half-chair-shaped, conformer (# 4, cf. Fig. 2b, on the left); it can be seen that certain hydrogen

bonds re-appear and reform for 0.1-1 ps and that there is usually always one instantaneous hydrogen bond present; in this case, six distinct hydrogen atoms attached to carbon atoms on the catalyst central ring, side benzyl groups and the benzene group. The probability distribution of the persistence times was found to be approximately Gaussian, in general. Transient hydrogen bonding was also detected between THF molecules in the AIMD simulations (using the same geometric definition as described above); however, the lack of a condensed phase of solvent molecules beyond the first solvation layer of only six THF molecules (the de facto 'upper limit' with the computational facilities and $O(N^3)$-scaling computational complexity) meant that such solvent-solvent hydrogen bonds formed very briefly. As discussed previously, AIMD under PBC with linear-scaling DFT would allow for a much more realistic definition of solvent-solvent hydrogen bonds.

[insert Figs. 2 and 3 about here]

The key variation in geometry between neglecting THF molecules to at least incorporating the first solvation layer of explicit THF molecules lies in an 'exaggerated' catalyst structure, featuring mainly phenyl rotation at the C-N bond, and the bond angle between the Ru-C-N (cf. Fig. 2b). Without solvent, gas-phase optimisation leads to the Ru-C-N bond angle being 128.8°, whereas in the explicit solvent (for the lowest-energy conformer, *i.e.*, # 4), this angle is 112.3°. The deviation of this bond angle can be understand clearly in that the nitrogen centre switches from a planar to a slightly deviated, or 'puckered', pyramidal shape, owing to interactions with THF. Without THF, the six-membered ring adopts an entirely planar form, whereas this is more 'half-chair-shaped' in explicit THF. In this conformation, bi-functional (Ru and N or –CH) groups are readily available for any kind of addition reactions. Reference to Fig. 2b shows that for configuration # 5 (that with the smallest-magnitude interaction energy), the six-membered ring is essentially boat-shaped, and the HC-Ru distance is somewhat shorter. Naturally, these distinct differences in conformation due to interactions with the solvent would be expected to lead to differences in chemical reactivity. Experimentally, the use of different solvents do have a profound effect on the reactivity of these classes of Ru-based catalysts.

In order to assess dynamical properties of the catalyst in the presence of explicit solvent, and contrast with a pure gas-phase treatment *sans* solvent, velocity autocorrelation functions

(VACFs) were extracted from the AIMD simulations of each atom type,[8] and their power spectra were calculated from Fourier (cosine) transformation. In the lowest-energy conformer (# 4) in particular, it was found that there was a sustained close contact between the positively-charged Ru atom and the oxygen atom of THF (cf. Fig. 4); this strong electrostatic interaction, in addition to other hydrogen bonds with the catalyst, led to a downshift in the gas-phase 120-190 cm^{-1} modes down to 40-75 cm^{-1}. In contrast, the conformation with the smallest-magnitude interaction energy (# 5) saw a decrease in the 280-300 cm^{-1} gas-phase mode down to 240-270 cm^{-1}. These shifts arise as a result of the distinct effect of different (solvent-mediated) conformations in Fig. 2b on the Ru vibrational states: the effect of the solvato-chromatic shift is to reduce the vibrational frequency of the Ru atom, as one would expect. Similarly, Fig. 5 depicts the power spectrum and VACF of the carbon atoms in the auxiliary benzene ring of the catalyst. Again, there is a more distinct difference for the boat-shaped conformation (in dashed grey, also cf. right panel of Fig. 2b) – this is especially evident in the underlying VACF and the enhancement of modes in 240-280 cm-1; velocity cross-correlation functions between the THF oxygen/carbon atoms and the catalyst heavy atoms, and their corresponding power spectra, also showed distinct trends of coupling. Shifts are also evident in Fig. 6 for the two nitrogen atoms in the central six-membered ring of the catalyst. In particular, the gas-phase peak at ~500 cm^{-1} is red-shifted down to ~420 and ~480 cm^{-1} in the half-chair and boat-shaped conformers of Fig. 2b; similarly, explicit solvation suppresses the low-frequency modes of 60-90 cm^{-1}, and gas-phase simulation fails to capture this subtlety. In Fig. 7, for the C atom in the CH moiety on the central six-membered ring, there is a very substantial red-shift from 500 to ~160 cm^{-1} upon explicit solvation in the half-chair-shaped configuration (# 4); in contrast, the somewhat weaker interaction with the solvent in the boat-shaped configuration (# 5) leads to the promotion of higher-frequency librational (rotation oscillation) and bond-angle-bending modes, due to higher-frequency interactions with a somewhat more distant solvent, with fewer hydrogen bonding interactions. Fig. 8, on the other hand, shows relatively little qualitative effect of explicit solvation on the vibrational modes of the ring-carbon atoms attached to the methyl groups; the smaller solvent-accessible surface area of these atoms leads to less scope for direct interaction with the solvent, as confirmed by examination of the relevant velocity cross-correlation functions with the THF.

[insert Figs. 4 to 8 about here]

Reaction Cycle

Having examined in some detail the effects of solvation upon one particular species (*i.e.*, catalyst structure **1** in Scheme **1**), it is perhaps appropriate to explore further explicit-solvation effects upon the catalytic cycle. To this end, we carried out classical MD simulations under PBC in THF (prepared and conducted exactly as before) of the ammonia-borane-addition transition state (**TS1**), the corresponding di-hydrogen intermediate (**3**) and the hydrogen-removal transition states (**TS2**); the reaction scheme is detailed in Scheme 1. As before, we sampled ten representative configurations of each of these three catalyst states with their immediate solvation layer for further DFT-optimisation and PM6-level ADMP simulation, in exactly the same manner as described above. We probed the structural, energetic and dynamical properties of both of these important transition states and the intermediate state, as well as interactions with the solvent. It was found that there was a rich variety of different placements and angular orientations of the THF molecules with respect to the transition states and intermediate 'scaffold', often governed by various different hydrogen-bonding arrangements. A selection of more representative configurations are shown in Fig. 9; here, we can observe clearly that explicit THF molecules affect the ammonia-borane conformation strongly through hydrogen bonding with –NH and –BH. In case of di-hydrogen intermediate **3**, the complex is stabilised strongly through a prominent hydrogen-bonding interaction with adjoining THF molecule; we assume that due to strong stabilisation of the di-hydrogen intermediate, the dehydrogenation process requires overcoming a larger activation-energy barrier to proceed. In the case of TS2@$(THF)_6$, there was found to be no real influence of the explicit THF solvent molecules on either of the hydrogen atoms of the dehydrogenation transition state; RMSDs vis-à-vis the gas-phase-optimised state (in the absence of explicit THF) were comparatively smaller.

The species-solvent interaction energies from classical MD were (computed as the sum of full van der Waals energy component under PBC and the Born electrostatic energy with continuum solvent, as in Table 1) -71.3 ± 2.2, -70.2 ± 2.0 and -57.6 ± 1.4 kcal/mol for **TS1**, **TS2** and the di-hydrogen intermediate (**3**). It can be seen that there is relatively little difference in the interaction energies (in total, and also for van der Waals and electrostatic component) for TS1 and T2 vis-à-vis structure 1 (~ -74 kcal/mol), due to their relative similarity (cf. Scheme 1 and Figs. 1 and 9), despite the structural (*i.e.*, configurational)

variety observed for species 1 in Fig. 2. However, it is clear that there is less energetic interaction between the intermediate structure 3 (cf. Scheme 1) and the solvent molecules, chiefly due to less van der Waals interaction, with less strong direct non-bonding interactions, such as hydrogen bonds. Upon examination of the AIMD-VACF spectra (along the lines of those presented in Figs. 4-8), it was found that there was less 'solvato-chromatic' red-shift for species **3**, in contrast to **TS1** and **TS2** which exhibited those similar to those observed for species **1** in Figs. 4-8. For instance, gas-phase Ru modes in the absence of solvent at 135-180 cm^{-1} were shifted down to 65-100 cm^{-1} in TS1 and TS2, but only to 95-130 cm^{-1} in intermediate structure **3**.

Concluding Remarks

Classical and *ab initio* MD has been carried out compare and contrast the effect of explicit and implicit solvation representation of THF on the structural, energetic and dynamical properties of a novel bifunctional arene ruthenium catalyst. It was found that the presence of explicit THF solvent molecules is required to capture an accurate picture of the catalyst's structural properties, particularly in view of the importance of hydrogen bonding with the surrounding THF molecules (cf. Fig. 2). Hydrogen bonding with the solvent was found to be very important at governing the structure, and the persistence times of individual bonds were determined; a rich variety of behaviour was observed in each of the ten AIMD simulations. Coupled with the lack of capacity of traditional O(N^3)-scaling DFT to handle sufficient number of solvent molecules to capture adequate dispersion interactions up to 8-10 Å from the catalyst (and apart from the accuracy of dispersion in the functional *per se*), this has serious negative implications on the accuracy of interaction (solvation) energies; the use of PCM may improve this somewhat from an electrostatic perspective, but the underlying structures and lack of a converged estimate of dispersion energy is a serious flaw. This is not to necessarily suggest that classical simulation is superior, given the inherent problems in appropriate parameterisation – it is not. However, its ability to allow for full-PBC treatment and size-convergence of the energetic (van der Waals) interactions is *sine qua non* for a more accurate *energetic* estimate (again, quite independent of underlying structural considerations); the use of Born or Poisson-Boltzmann electrostatics on explicitly-solvated configurations is (arguably) optimal and to be encouraged;[34] naturally, the use of implicit solvation to generate the configurations in the first place is (arguably grossly) incorrect, whether by MD or other

methods. The use of PBC implementations of linear-scaling, dispersion-corrected DFT[10] to generate realistic configurations, *e.g.*, via AIMD, with sufficient numbers of atoms to achieve essentially size-independent structures and converged interaction energies is an important goal for future progress in this area.

Acknowledgements

The authors thank Drs. Andrew Phillips and Nitin Wadnerkar for useful discussions. This material is based upon works supported by Science Foundation Ireland (SFI) under Grant No. [07/SRC/B1160]. We thank SFI for the provision of high-performance computing facilities.

References

1) Berthelot, M.; St.Gilles, L.P. (a) RECHERCHES SUR LES AFFINITES. DE LA formation et de la decomposition des ethers *Ann.Chim.Phys* 3 ser **1862**, *65*, 385 (b) **1862**, *66*, 5 and **1863**, *68*, 225.

2) Zaugg, H. E. Specific Solvent Effects in the Alkylation of Enolate Anions. II. Relationships between Structure and Physical Properties of Additives and Their Catalytic Efficiencies. *J. Am. Chem. Soc*., **1960**, *82*, 2903–2909.

3) (a) Miertus, S.; Scrocco, E.; Tomasi. Electrostatic interaction of a solute with a continuum. A direct utilizaion of AB initio molecular potentials for the prevision of solvent effects. *Chem. Phys.* **1981**, *55*, 117. (b) Cammi, R.; Tomasi, J. Remarks on the use of the apparent surface charges (ASC) methods in solvation problems: Iterative versus matrix-inversion procedures and the renormalization of the apparent charges. *J. Comput. Chem*. **1995**, *16*, 1449-1458.

4) (a) Klamt, A.; Schurmann, G. COSMO: a new approach to dielectric screening in solvents with explicit expressions for the screening energy and its gradient. *J. Chem. Soc., Perkin Trans. 2*, **1993**, 799-806. (b) Andzelm, J.; Kölmel, C.; Klamt, A. Incorporation of solvent effects into density functional calculations of molecular energies and geometries *J. Chem. Phys.* **1995**, *103*, 9312-9320.

5) Fogolari, F.; Brigo, A.; Molinari, H. The Poisson–Boltzmann equation for biomolecular electrostatics: a tool for structural biology . *J. Molec. Recognit.* **2002**, *15*, 377-392.

6) Onufiev, A.; Bashford, D.; Case, D.A. Effective Born radii in the generalized Born approximation: The importance of being perfect. *J. Comput. Chem.* **2002**, *23*, 1297-1304.

7) Zagrovic, B.; Pande, V. Solvent viscosity dependence of the folding rate of a small protein: Distributed computing study. *J. Comput. Chem.* **2003,** *24*, 1432-1436.

8) Allen, M.P.; Tildesley, D. J. *Computer Simulation of Liquids*, Oxford, **1987**.

9) (a) Warshel, A.; Levitt, M. Theoretical Studies of Enzymic Reactions : Dielectric, Electrostatic and Steric Stabilization of the Carbonium Ion in the Reaction of Lysozyme *J. Mol. Biol.* **1976**, *103*, 227-249. (b) Field, M. J.; Bash, P. A.; Karplus, M. A combined quantum mechanical and molecular mechanical potential for molecular dynamics simulations. *J. Comput. Chem*. **1990**, *11*, 700-733.

10) El-Hendawy, M. M.; English, N.J.; Mooney, D.A. A theoretical thermodynamic investigation of cascade reactions in dinuclear octa-azacryptates involving carbon dioxide. *J. Molec. Model*. **2013**, *17*, 3151-3162.

11) (a) Grubbs, R. H.; Burk, P. L.; Carr, D. D. Mechanism of the olefin metathesis reaction. *J. Am. Chem. Soc*. **1975**, *97*, 3265-3267. (b) Dias, E. L.; Nguyen, S.-B. T.; Grubbs, R. H. Well-Defined Ruthenium Olefin Metathesis Catalysts: Mechanism and Activity. *J. Am. Chem. Soc*. **1997**, *119*, 3887-3897. (c) Vougioukalakis, G. C.; Grubbs. R. H. Ruthenium-Based Heterocyclic Carbene-Coordinated Olefin Metathesis Catalysts. *Chemical Reviews*, **2010**, *110*, 1746-1787.

12) Schreiber, D. F.; O'Connor, C.; Grave, C.; Ortin, Y.; Müller-Bunz, H.; Phillips, A. D. Application of β-Diketiminato Arene-Substituted Ru(II) Complexes in Highly Efficient H_2 Dehydrocoupling of Amine Boranes. *ACS Catal*. **2012**, *2*, 2505-2511.

13) Blaquiere, N.; Diallo-Garcia, S.; Gorelsky, S. I.; Black, D. A.; Fagnou, K. Ruthenium-Catalyzed Dehydrogenation of Ammonia Boranes. *J. Am. Chem. Soc.* **2008**, *130*, 14034-14035.

14) Alcaraz, G.; Vendier, L.; Clot, E.; Sabo-Etienne, S. Ruthenium Bis(σ-B-H) Aminoborane Complexes from Dehydrogenation of Amine–Boranes: Trapping of H_2B-NH_2. *Angew. Chem.,Int. Ed*. **2010**, *49*, 918-920.

15) Boulho, C.; Djukic, J.-P. The dehydrogenation of ammonia-borane catalysed by dicarbonylruthenacyclic(II) complexes. *Dalton Trans*. **2010**, *39*, 8893-8905.

16) MacInnis, M. C.; McDonald, R.; Ferguson, M. J.; Tobisch, S.; Turculet, L. Four-Coordinate, 14-Electron RuII Complexes: Unusual Trigonal Pyramidal Geometry Enforced by Bis(phosphino)silyl Ligation. *J. Am. Chem. Soc.* **2011**, *133*, 13622-13633.

17) Conley, B. L.; Guess, D.; Williams, T. J. A Robust, Air-Stable, Reusable Ruthenium Catalyst for Dehydrogenation of Ammonia Borane. *J. Am. Chem. Soc.* **2011**,*133*, 14212-14215.

18) Wallis, C. J.; Dyer, H.; Vendier, L.; Alcaraz, G.; Sabo-Etienne, S. Dehydrogenation of Diamine–Monoboranes to Cyclic Diaminoboranes: Efficient Ruthenium-Catalyzed Dehydrogenative Cyclization. *Angew. Chem., Int. Ed.* **2012**, *51*, 3646.

19) Lide. D.R. CRC Handbook of Chemistry and Physics, 90th ed. **2009**, CRC Press.

20) MOE: The Molecular Operating Environment from Chemical Computing Group Inc., 1010 Sherbrooke St. W., Suite 910, Montréal, Québec, Canada H3A 2R7.

21) Cornell, W.D.; Cieplak, P.; Bayly, C.I.; Gould, I.R.; Merz Jr, K. M.; Ferguson, D.M. Spellmeyer, D.C.; Fox, T. Caldwell, J.W. Kollman, P.A. A Second Generation Force Field for the Simulation of Proteins, Nucleic Acids, and Organic Molecules. *J. Am. Chem. Soc*. **1995**, *117*, 5179-5197.

22) van Gunsteren, W.F.; Berendsen, H.J.C. Computer Simulation of Molecular Dynamics: Methodology, Applications, and Perspectives in Chemistry, *Angew. Chem., Int. Ed.* **1990,** *29*, 992-1023.

23) Neumann, M. The dielectric constant of water. Computer simulations with the MCY potential. *J. Chem. Phys*, **1985**, *82*, 5663-5672.

24) Izaguirre, J.A.; Reich, S.; Skeel, R.D. Longer time steps for molecular dynamics. *J Chem Phys*, **1999**, *110*, 9853-9864.

25) Zhao, Y.; Truhlar, D. G. Density Functionals with Broad Applicability in Chemistry. *Acc. Chem. Res*. **2008**, *41*, 157-167.

26) Zhao, Y.; Truhlar, D. G. The M06 suite of density functionals for main group thermochemistry, thermochemical kinetics, noncovalent interactions, excited states, and transition elements: two new functionals and systematic testing of four M06-class functionals and 12 other functionals. *Theor. Chem. Acc*. **2008**, *120*, 215-241.

27) Gaussian 09, Revision A.1, Frisch, M. J.; Trucks, G. W.; Schlegel, H. B.; Scuseria, G. E.; Robb, M. A.; Cheeseman, J. R.; Scalmani, G.; Barone, V.; Mennucci, B.; Petersson, G. A.; Nakatsuji, H.; Caricato, M.; Li, X.; Hratchian, H. P.; Izmaylov, A. F.; Bloino, J.; Zheng, G.; Sonnenberg, J. L.; Hada, M.; Ehara, M.; Toyota, K.; Fukuda, R.; Hasegawa, J.; Ishida, M.; Nakajima, T.; Honda, Y.; Kitao, O.; Nakai, H.; Vreven, T.; Montgomery, Jr., J. A.; Peralta, J. E.; Ogliaro, F.; Bearpark, M.; Heyd, J. J.; Brothers, E.; Kudin, K. N.;

Staroverov, V. N.; Kobayashi, R.; Normand, J.; Raghavachari, K.; Rendell, A.; Burant, J. C.; Iyengar, S. S.; Tomasi, J.; Cossi, M.; Rega, N.; Millam, N. J.; Klene, M.; Knox, J. E.; Cross, J. B.; Bakken, V.; Adamo, C.; Jaramillo, J.; Gomperts, R.; Stratmann, R. E.; Yazyev, O.; Austin, A. J.; Cammi, R.; Pomelli, C.; Ochterski, J. W.; Martin, R. L.; Morokuma, K.; Zakrzewski, V. G.; Voth, G. A.; Salvador, P.; Dannenberg, J. J.; Dapprich, S.; Daniels, A. D.; Farkas, Ö.; Foresman, J. B.; Ortiz, J. V.; Cioslowski, J.; Fox, D. J. Gaussian, Inc., Wallingford CT, 2009.

28) Nicklass, A.; Dolg, M.; Stoll, H.; Preuss, H. *Ab initio* energy- adjusted pseudopotentials for the noble gases Ne through Xe: Calculation of atomic dipole and quadrupole polarizabilities. *J. Chem. Phys*. **1995**, *102*, 8942-8952.

29) Schlegel, H. B. Millam, J. M. Iyengar, S. S. Voth, G. A. Daniels, A. D. Scuseria, G. E. Frisch, M. J. *Ab initio* molecular dynamics: Propagating the density matrix with Gaussian orbitals *J. Chem. Phys*. **2001**, *114*, 9758-9763.

30) Iyengar, S. S.; Schlegel, H. B.; Millam, J. M. Voth, G. A. Scuseria, G. E. Frisch, M. J. *Ab initio* molecular dynamics: Propagating the density matrix with Gaussian orbitals. II. Generalizations based on mass-weighting, idempotency, energy conservation and choice of initial conditions. *J. Chem. Phys*., **2001**, *115*, 10291-10302.

31) Schlegel, H. B.; Iyengar, S. S.; Li, X.; Millam, J. M.; Voth, G. A.; Scuseria, G. E.; Frisch, M. J. *Ab initio* molecular dynamics: Propagating the density matrix with Gaussian orbitals. III. Comparison with Born–Oppenheimer dynamics. *J. Chem. Phys*., **2002**, *117*, 8694-8704.

32) Iyengar, S. S.; Schlegel, H. B.; Millam, J. M.; Voth, G. A. Scuseria, G. E. Frisch, M. J. Ab initio molecular dynamics: Propagating the density matrix with gaussian orbitals. IV. Formal analysis of the deviations from Born-Oppenheimer dynamics. *Israel J. Chem.* **2002**, *7*, 191-202. (e) S. S. Iyengar and M. J. Frisch, Effect of time-dependent basis functions and their superposition error on atom-centered density matrix propagation (ADMP): Connections to wavelet theory of multiresolution analysis. *J. Chem. Phys*., **2004**, *121*, 5061-5070.

33) Stewart, J. J. P. Optimization of parameters for semiempirical methods V: Modification of NDDO approximations and application to 70 elements. *J. Mol. Model*. **2007**, *13*, 1173-1213.

34) English, N. J. Calculation of binding affinities of HIV-1 RT and β-secretase inhibitors using the linear interaction energy method with explicit and continuum solvation approaches. *J. Mol. Model.*, **2007**, *13*, 1081-1097.

Table 1. van der Waals and Coulombic interaction energy components (kcal/mol), with totals thereof. '(6)' denotes the components and total for interactions with the six nearest THF molecules (on a non-PBC basis), whilst PBC refers to interactions with all THF molecules in the simulation box on a PBC basis. Reaction field electrostatics is used in both cases. 'Born' refers to the electrostatic component of the interaction energy of the solute with the Generalised Born implicit solvent (with the THF molecules stripped away).

Conf	vdW (6)	Coul (6)	Tot (6)	vdW_{PBC}	$Coul_{PBC}$	Tot_{PBC}	Born	vdW_{PBC}+Born
1	-4.23	-46.5	-50.7	-24.2	-78.5	-102.7	-48.9	-73.1
2	-4.45	-48.7	-53.2	-24.8	-80.2	-105.0	-49.5	-74.3
3	-5.71	-48.3	-54.0	-25.4	-81.4	-106.8	-48.7	-74.1
4	-5.85	-48.6	-54.5	-25.9	-82.3	-108.2	-50.1	-76.0
5	-5.13	-46.8	-51.9	-23.3	-79.4	-102.7	-50.2	-73.5
6	-4.64	-46.3	-50.9	-22.9	-77.6	-100.5	-49.6	-72.5
7	-3.97	-45.7	-49.7	-23.8	-80.7	-104.5	-48.1	-71.9
8	-4.18	-44.4	-48.6	-25.0	-78.6	-103.6	-49.4	-74.4
9	-4.83	-48.9	-53.7	-23.7	-77.2	-100.9	-49.6	-73.3
10	-5.32	-47.3	-52.6	-24.6	-81.0	-105.6	-48.2	-72.8

Table 2. Interaction energies (kcal/mol) and RMSDs of the catalyst vis-à-vis the lowest-energy configuration (# 4); note that these configurations (with the six THF molecules) have been optimised *in vacuo* using the classical MD snapshots as starting points. In both cases (i.e., gas-phase and with the PCM approach), single-point energy calculations were undertaken on the gas-phase-optimised configurations; the interaction energy was computed by subtracting the energies of the separate assemblies of THF and catalyst from that of the solute-THF complex.

Config.	IE^a	IE^b	RMSD (Å)
1	-69.94	-49.81	1.42
2	-51.72	-35.74	2.19
3	-51.84	-35.52	1.83
4	**-84.82**	**-61.48**	**0.0**
5	-44.52	-27.91	2.22
6	-46.21	-30.85	2.25
7	-45.43	-29.78	2.13
8	-67.92	-48.53	1.44
9	-45.63	-31.99	2.23
10	-58.18	-38.10	1.96

-a- Interaction energies of catalyst and THF solvent (gas-phase), kcal/mol
-b- Interaction energies of catalyst and THF solvent (PCM), kcal/mol

Figure list

Scheme 1: Catalytic cycle for dehydrogenation of AB (**a**) with Ru-catalyst (**1**)

Figure 1: Gas-phase optimised configurations of bifunctional arene ruthenium catalyst with the six surrounding THF molecules. Hydrogen-bonding contacts are illustrated by the red lines.

Figure 2: (a) Gas-phase optimised configuration without solvent; (b) Optimised solvated configurations with largest and smallest-magnitude interaction energies – the half-chair-shaped one on the left is the largest-magnitude in interaction energy (# 4), whilst the boat-shaped one on the right is the lowest-magnitude (# 5).

Figure 3: Typical time-evolution of hydrogen bonding patterns of a single THF molecule's oxygen atom with six distinct H atoms attached to carbon atoms on the catalyst central ring, side benzyl groups and the benzene group. The repeated establishment and disappearance of hydrogen bonds is apparent.

Figure 4: Normalised power spectrum of the VACF of Ru. Continuous black represents AIMD without any solvent in the gas-phase, whilst the black dotted line represents the lowest-energy (or largest-interaction energy magnitude) system (# 4), and the dashed grey line the smallest-magnitude interaction energy system (# 5).

Figure 5: Normalised power spectrum of the VACF of the carbon atoms in the auxiliary benzene ring of the catalyst. See caption of Fig. 4 for a description of the symbols. The inset in the top-right depicts the underlying VACFs.

Figure 6: Normalised power spectrum of the VACF of the nitrogen atoms in the catalyst. Line types as in Fig. 4.

Figure 7: Normalised power spectrum of the carbon atom in the catalyst's central six-membered ring attached to the single hydrogen atom. Line types as in Fig. 4.

Figure 8: Normalised power spectrum of the carbon atoms in the catalyst's central six-membered ring attached to a methyl group. Line types as in Fig. 4.

Figure 9: DFT-optimised configurations of ammonia-borane-addition transition state, di-hydrogen intermediate and hydrogen removal transition states with the six surrounding THF molecules (done under gas-phase conditions). Hydrogen-bonding contacts are illustrated by the black lines.

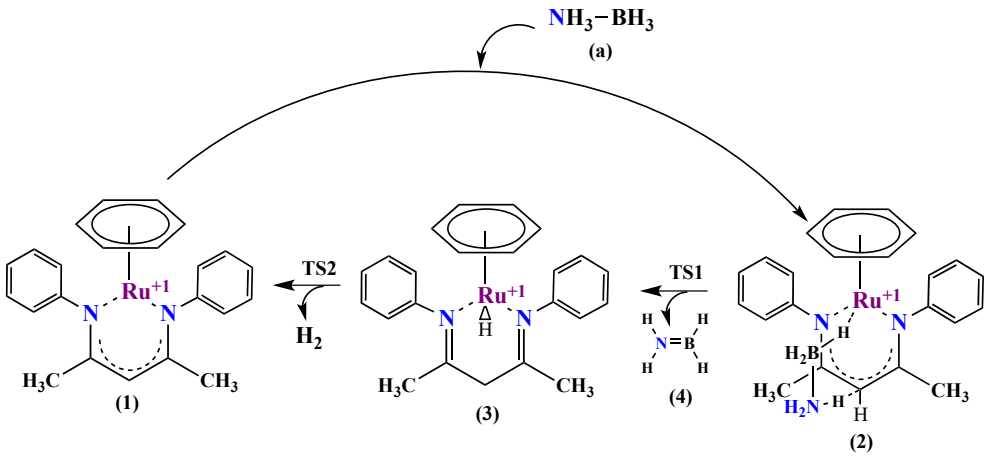
NH3−BH3
(a)
Ru+1
N
N
H3C
CH3
(1)
TS2
H2
Ru+1
N
H
N
H3C
CH3
(3)
TS1
H
N=B
H
H
H
(4)
Ru+1
N
H
N
H2B
H3C
H2N
H
CH3
H
(2)

Scheme 1

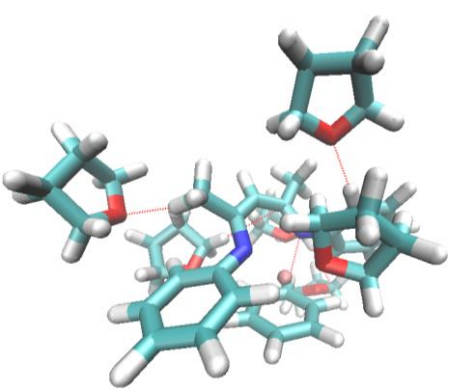

Conf 1

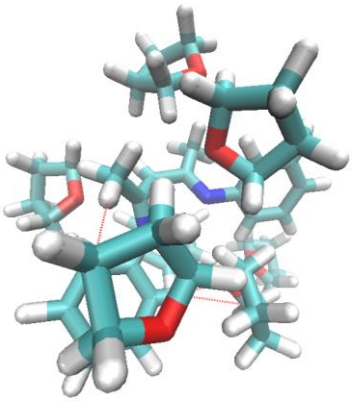

Conf 2

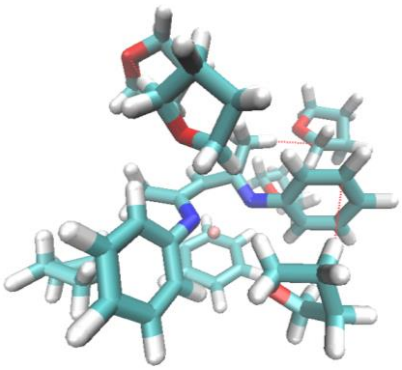

Conf 3

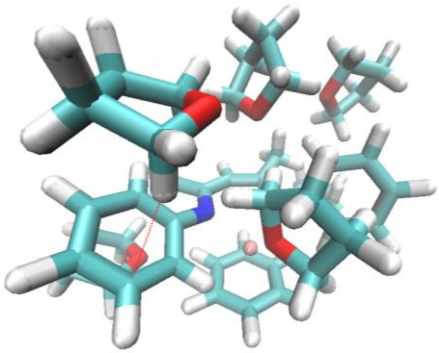

Conf 4

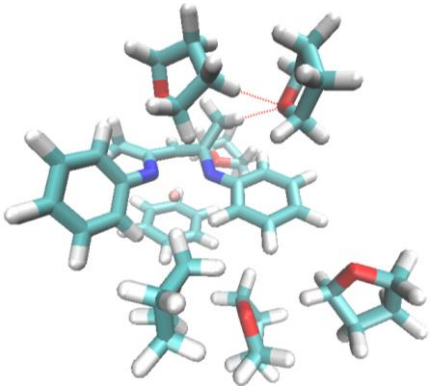

Conf 5

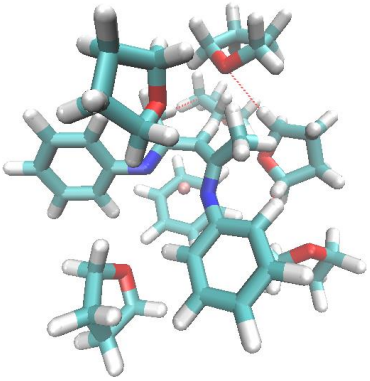

Conf 6

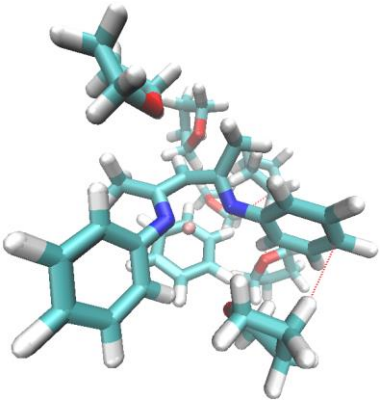

Conf 7

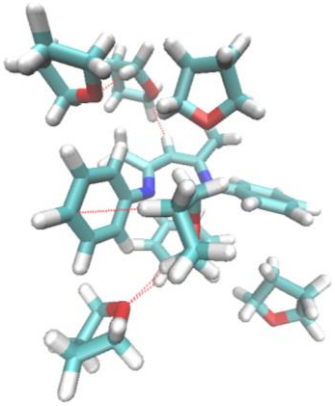

Conf 8

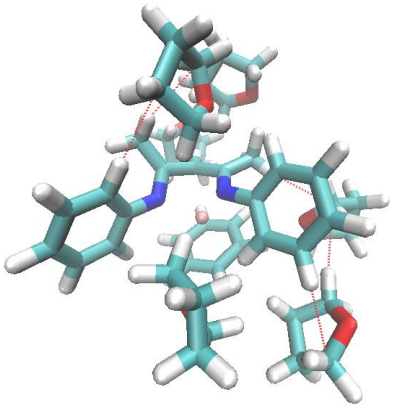

Conf 9

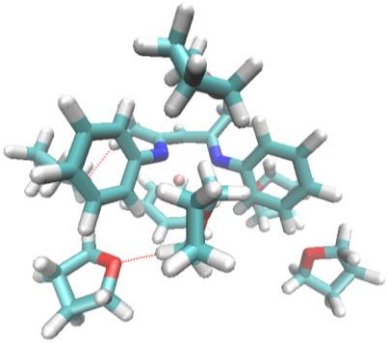

Conf 10

Figure 1

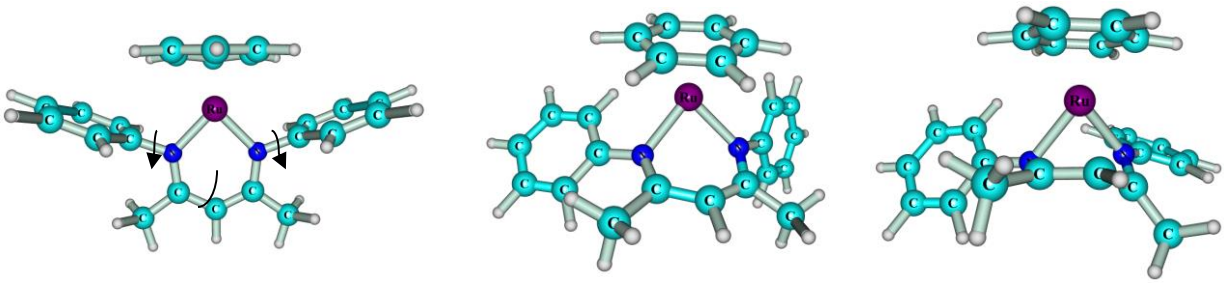

Gas-phase-optimised

(a)

Half chair-shaped

Boat-shaped

(b)
With explicit solvent

Figure 2

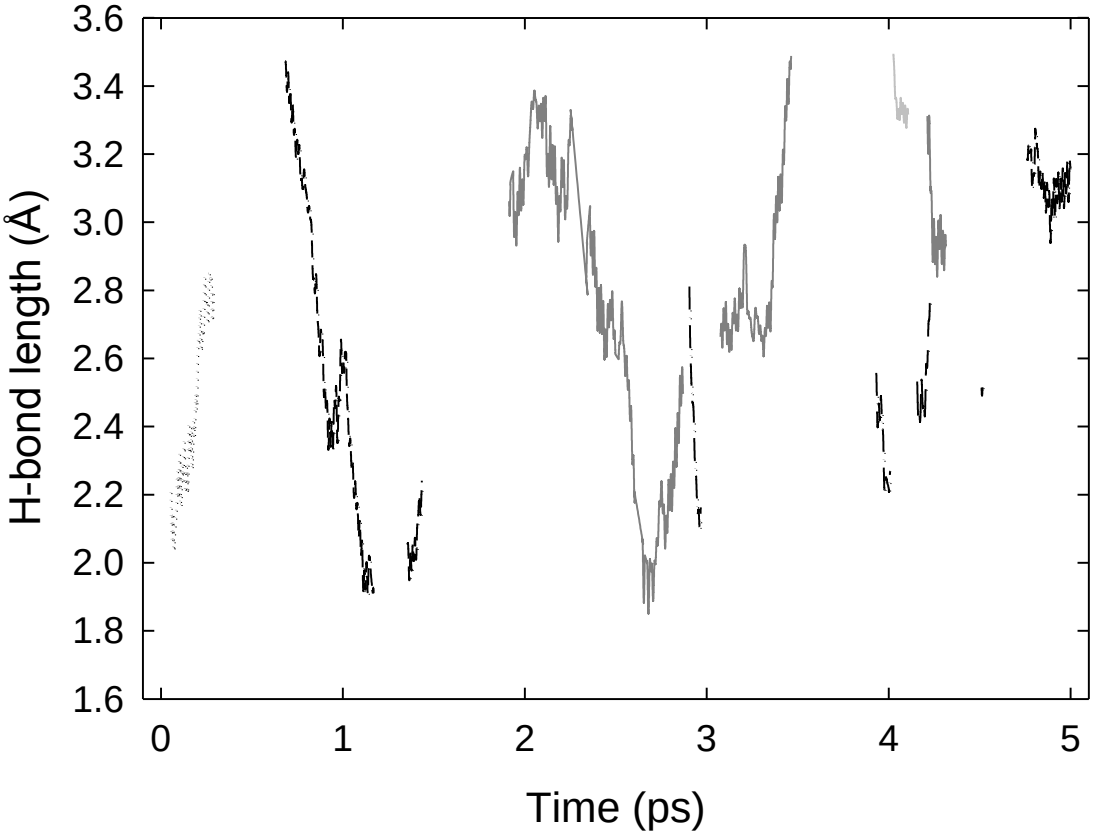

Fig. 3

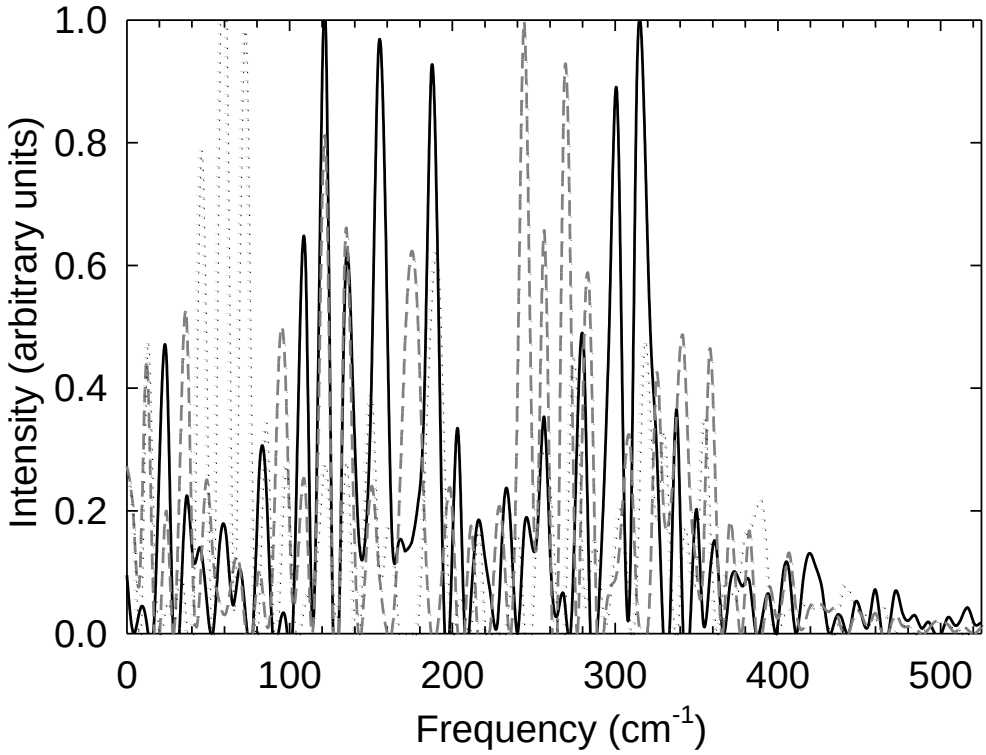
1.0
0.8
0.6
0.4
0.2
0.0
Intensity (arbitrary units)
0
100
200
300
400
500
Frequency (cm-1)

Fig. 4

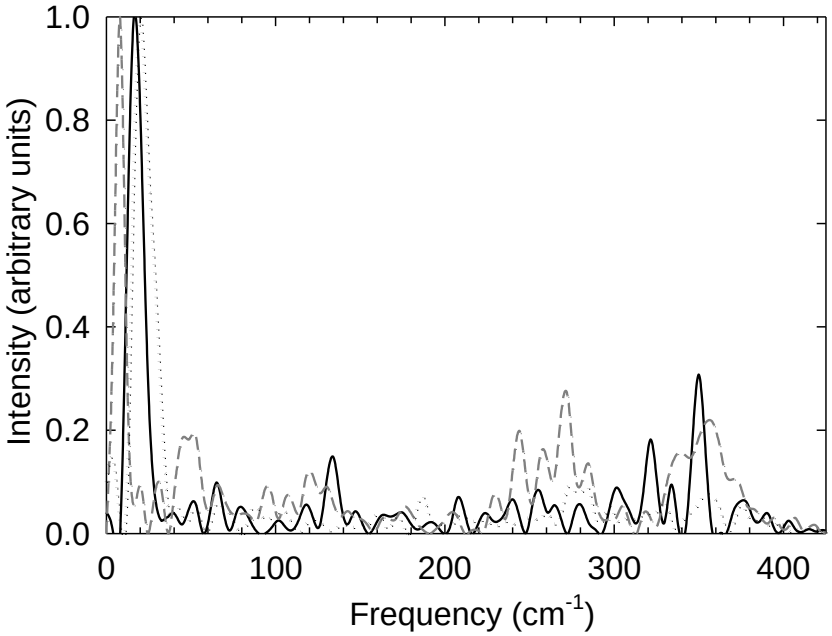

Fig. 5 (above)

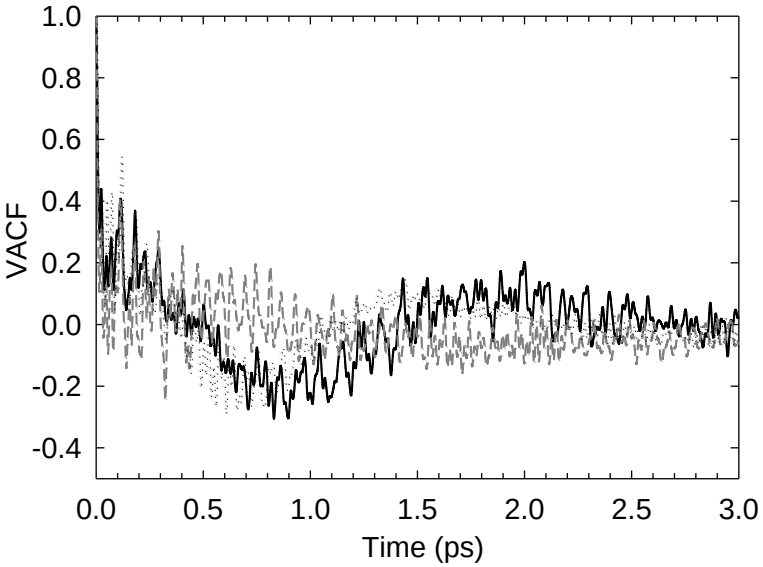

Fig. 5 (inset to be placed in the top-right of the graph on the top of the page)

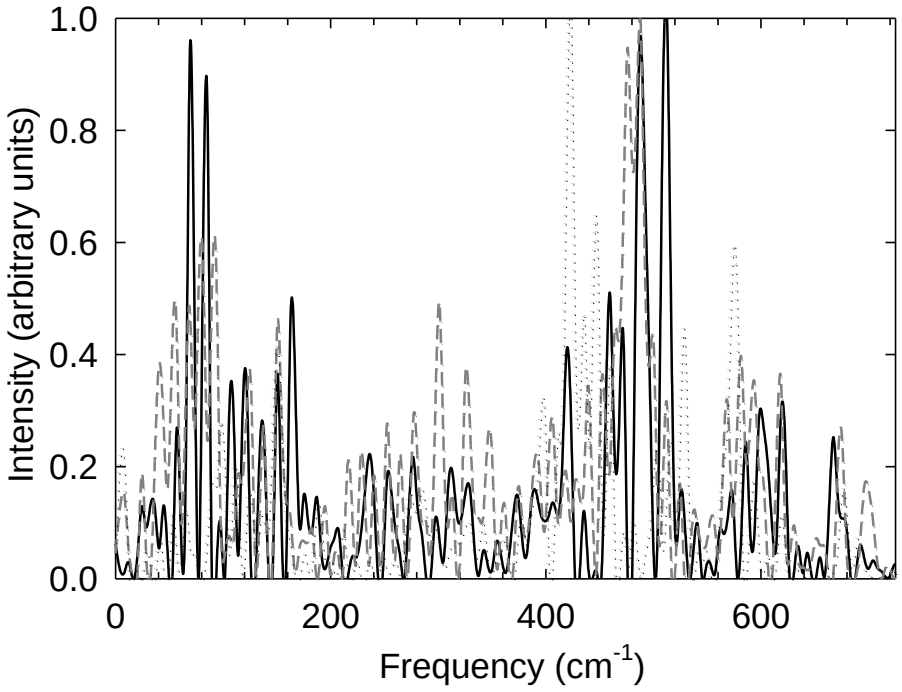
1.0
0.8
0.6
0.4
0.2
0.0
Intensity (arbitrary units)
0
200
400
600
Frequency (cm-1)

Fig. 6

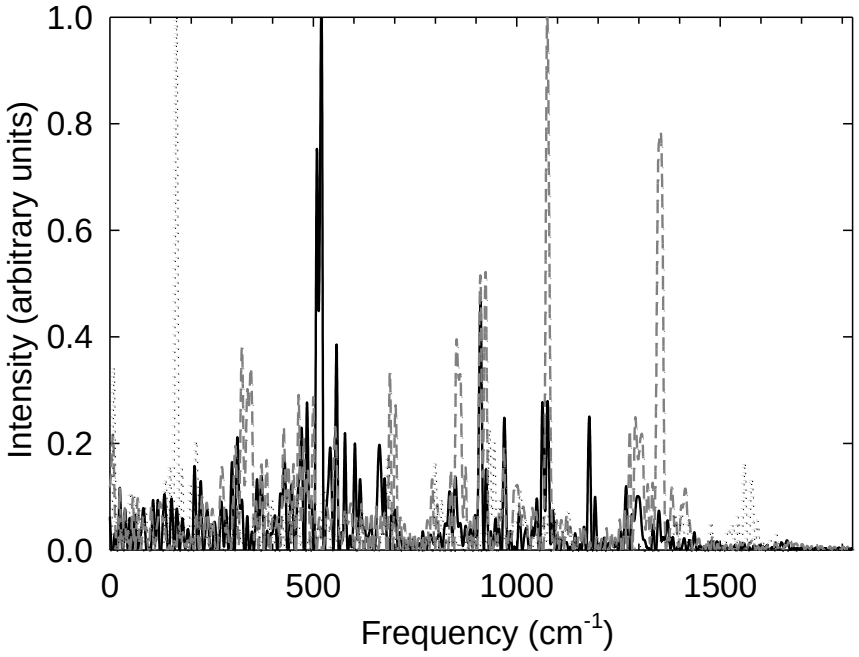
1.0
0.8
0.6
0.4
0.2
0.0
Intensity (arbitrary units)
0
500
1000
1500
Frequency (cm-1)

Fig. 7

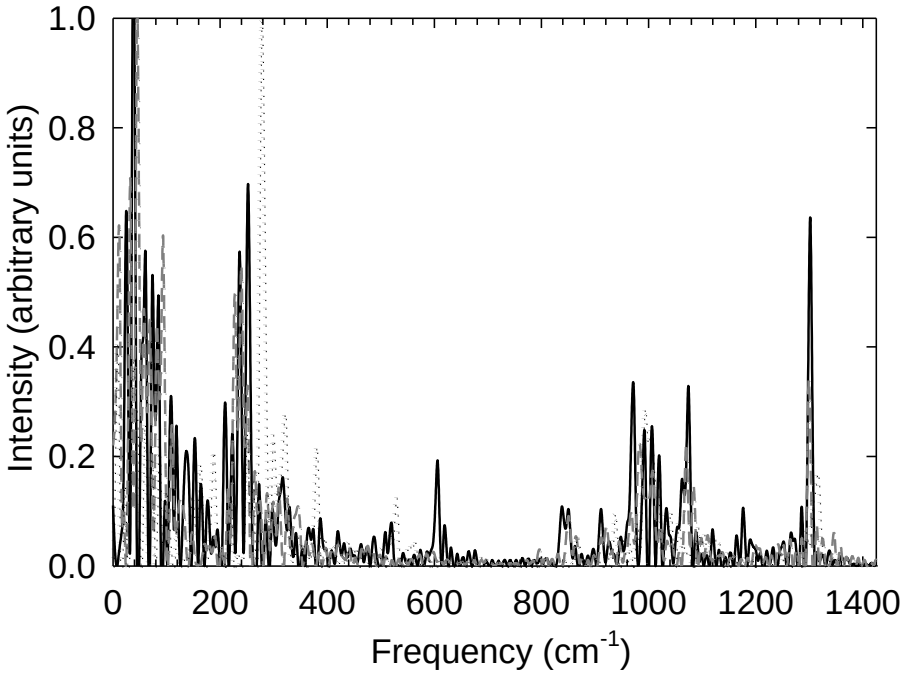
1.0
0.8
0.6
0.4
0.2
0.0
Intensity (arbitrary units)
0
200
400
600
800
1000
1200
1400
Frequency (cm-1)

Fig. 8

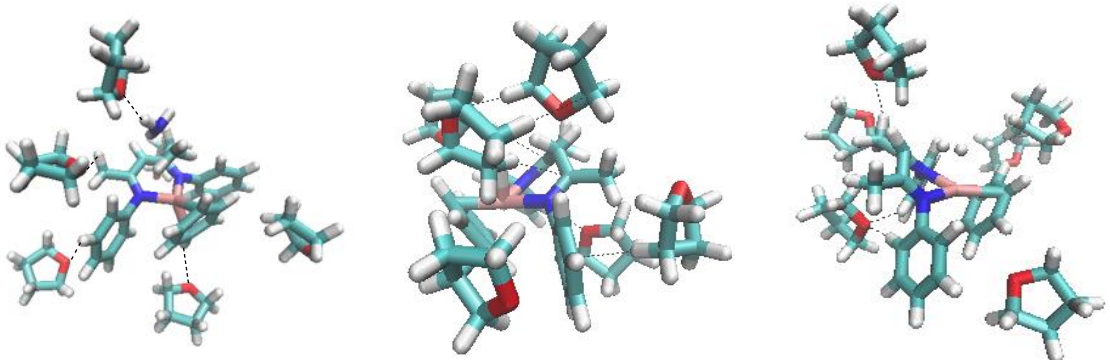

TS1@(THF)$_6$ **3@(THF)$_6$** **TS2@(THF)$_6$**

Fig. 9